Supplementary Information: Shock formation and rate effects in impacted carbon nanotube foams

*Ramathasan Thevamaran[1,2], Eric R. Meshot[3], Chiara Daraio[1,2,]**

[1]Division of Engineering and Applied Sciences, California Institute of Technology, Pasadena, CA, USA.

[2]Dept. of Mechanical and Process Engineering, Swiss Federal Institute of Technology Zurich (ETH Zurich), Switzerland.

[3]Physical and Life Sciences Directorate, Lawrence Livermore National Laboratory, Livermore, CA, USA.

*Corresponding author: daraio@ethz.ch

[S1]. Intrinsic density and alignment characterization: Methods.

We performed synchrotron X-ray scattering and mass attenuation measurements to nondestructively quantify the density and alignment within VACNT foams. A beam energy of 10 keV was selected with a Mo/B_4C double multilayer monochromator, and the height of the beam-spot was less than 300 µm at the sample with a measured flux of 10^{12} photons sec^{-1}. The VACNT sample was mounted on a motorized stage that enables 1) tilt alignment to make the sample's Si substrate parallel to the X-ray beam as well as 2) spatial mapping of the structural characteristics of the sample along its height.

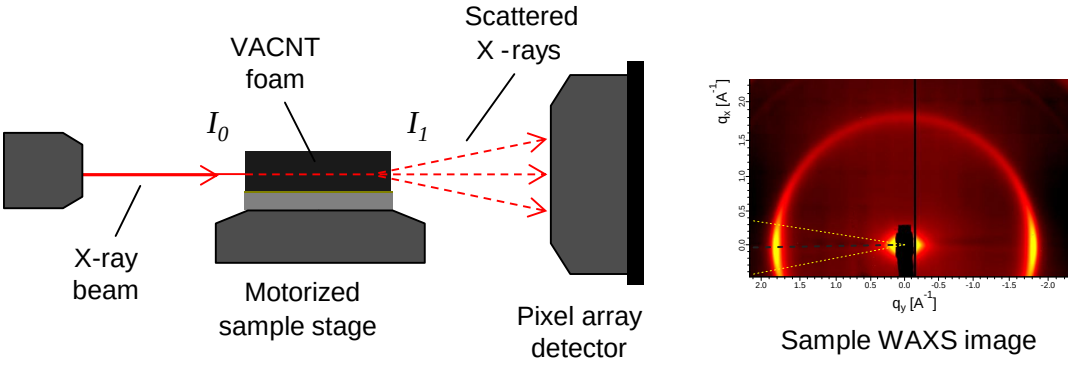

Figure S1. Schematic side view of the experimental setup for X-ray characterization with a representative WAXS image collected from our VACNT foams. The x-z-α stage enables spatial mapping and alignment of the VACNT to the X-ray beam, and the scattered X-rays are collected on a Pilatus 1M pixel detector.

We monitored the X-ray intensity upstream (I_0) and downstream (I_1) of the sample by measuring ion current at the locations denoted in the schematic. These values were used to calculate the mass density of the sample based on the Beer-Lambert law [1],

$$\rho_{CNT} = \frac{\ln\left(I_0/I_1\right)}{t\left(\mu/\rho\right)}, \tag{1}$$

where ρ_{CNT} is the VACNT volumetric mass density, t is the path-length through the VACNT, and (μ/ρ) is the mass attenuation coefficient. Values for (μ/ρ) are tabulated by NIST as a function of element and X-ray energy, and we used a weighted average between C and Fe, because our floating-catalyst synthesis process deposits small quantities of Fe, which we measured to be approximately 5% by energy-dispersive X-ray spectroscopy (EDX) in scanning electron microscope (SEM).

$$\left(\mu/\rho\right) = (1-w)\left(\mu/\rho\right)_C + w\left(\mu/\rho\right)_{Fe}, \tag{2}$$

where w is the weight fraction of Fe.

[S2]. Intrinsic density and alignment characterization: Results.

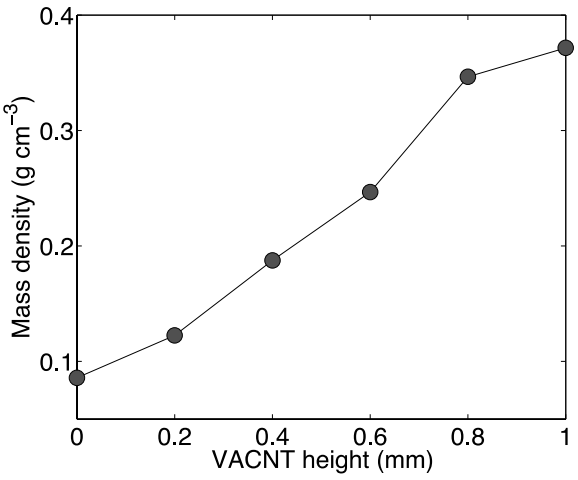

Figure S2(a). Characteristic intrinsic density variation along the height of the VACNT from the substrate. Zero is where the bottom of the beam meets silicon substrate. The sample was synthesized using 5% H_2 concentration (measured mean density 0.23 gcm^{-3}).

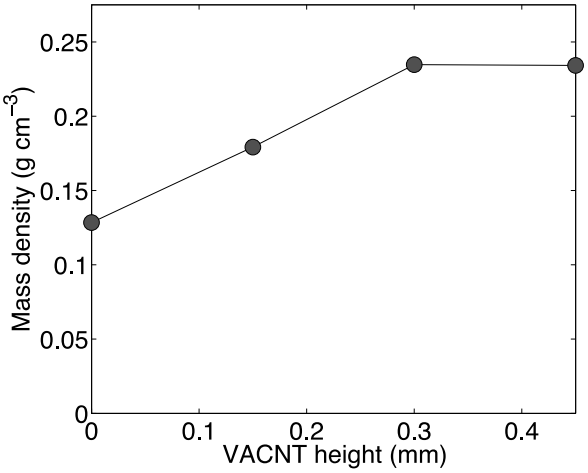

Figure S2(b). Characteristic intrinsic density variation along the height of the VACNT from the substrate. Zero is where the bottom of the beam meets silicon substrate. The sample was synthesized using 15% H_2 concentration (measured mean density 0.19 gcm^{-3}).

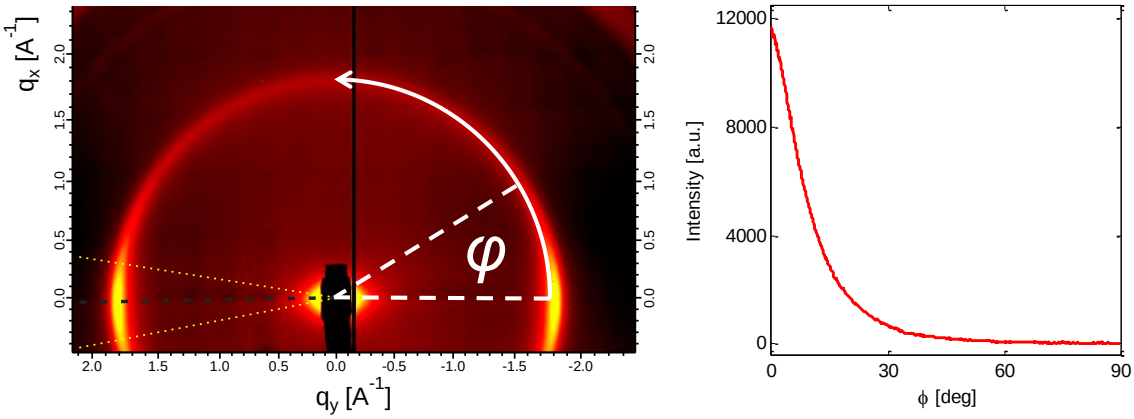

Figure S2(c). Schematic illustration demonstrates the azimuthal integration we perform on WAXS images to extract the Hermans orientation factor. The annulus of integration is define by ±5 pixels from the diffraction peak located at q = 1.8 Å^{-1}, which corresponds to scattering from the concentric shells of multiwall CNTs.

In addition to measuring the X-ray attenuation, we also quantified the average CNT alignment from the anisotropy of wide-angle X-ray scattering (WAXS) patterns. Using the distribution of scattered intensity about the azimuthal angle φ, we calculated the Herman's orientation factor [2,3],

$$f = \frac{1}{2}(3\langle\cos^2\varphi\rangle - 1). \quad (3)$$

Here, f equals 1 for perfectly aligned CNTs and 0 for random order (no alignment), and

$$\langle\cos^2\varphi\rangle = \frac{\int_0^{\pi/2} d\varphi\, I(\varphi)\sin\varphi\cos^2\varphi}{\int_0^{\pi/2} d\varphi\, I(\varphi)\sin\varphi}. \quad (4)$$

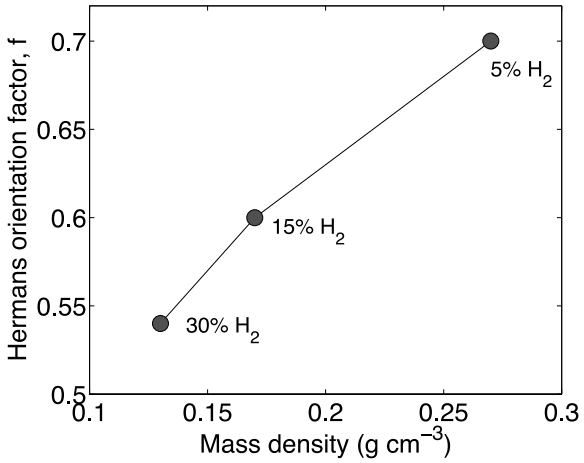

Figure S2(d). Direct correlation of alignment (*f*) with the mass density of VACNTs synthesized under the H_2 conditions in this study (5%, 15%, 30% concentration). Results from previous studies would suggest that this is a sublinear correlation, with *f* rapidly dropping to zero once a lower threshold in CNT density is reached [1].

[S3]. Definition of parameters

Stress: The nominal stress (engineering stress) experienced by the specimen during impact, calculated by,

$$\sigma = \frac{F}{A}, \quad (5)$$

where *F* is the impact force measured by the dynamic force sensor and *A* is the initial area of the VACNT foam specimen.

Strain: The nominal strain (engineering strain) on the specimen, calculated by,

$$\varepsilon = \frac{\delta}{H}, \tag{6}$$

where δ is the dynamic displacement measured using the moiré interferometer and H is the initial height of the specimen.

Strain-rate: The effective strain rate at the moment of impact, given by,

$$\dot{\varepsilon} = \frac{V_{impact}}{H}, \tag{7}$$

where V_{impact} is the initial rate of deformation and H is the initial height of the specimen.

Unloading modulus: The gradient of the unloading curve on the stress-strain diagram at the beginning of unloading. It was calculated by,

$$E_{unloading} = \frac{\sigma(\varepsilon_{max}) - \sigma(0.95\ \varepsilon_{max})}{(\varepsilon_{max} - 0.95\ \varepsilon_{max})}, \tag{8}$$

where ε_{max} is the maximum strain attained during impact and $\sigma(\varepsilon_{max})$ denotes the stress corresponding to the ε_{max}.

Recovery: Percentage recovery of the specimen during unloading calculated by,

$$Percentage\ Recovery = \frac{\varepsilon_{max} - \varepsilon_f}{\varepsilon_{max}} \times 100. \tag{9}$$

Energy Dissipated: The hysteretic energy dissipation given by the area included within the hysteretic loop on the dynamic stress-strain diagram [Figure S3(a)].

$$W_{dissipated} = \oint \sigma\ d\varepsilon. \tag{10}$$

Dynamic cushion factor: The factor representing the damping characteristic of the VACNT foam. It was calculated by,

$$C_{dyn} = \frac{\sigma_p}{W_p}, \tag{11}$$

where σ_p is the peak stress and W_p is the energy absorbed up to the peak stress (Figure S3(b)) given by,

$$W_p = \int_0^{\sigma_p} \sigma \, d\varepsilon. \tag{12}$$

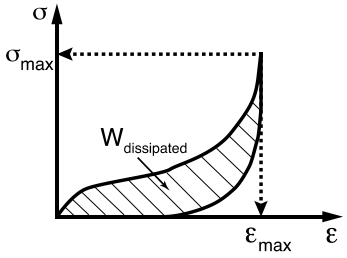

Figure S3(a). Energy dissipated

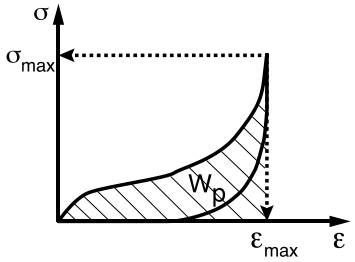

Figure S3(b). Energy absorbed up to peak stress

Definition of shock parameters:

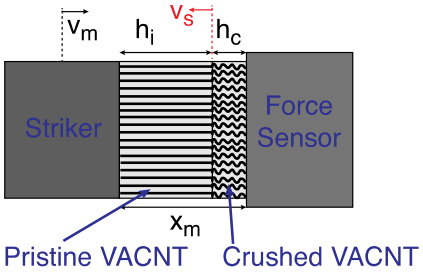

Figure S3(c). Shock formation of VACNT foams

Striker velocity: The velocity at which the striker compresses the VACNT foam, defined by,

$$v_m = \frac{\Delta x_m}{\Delta t}, \tag{13}$$

where x_m is the current thickness of the VACNT foam. It is equivalent to the particle velocity of the intact VACNT foam in the case of a direct impact.

Crush front velocity: The velocity at which the sharp crush front progresses towards the striker, defined by,

$$v_c = \frac{\Delta h_c}{\Delta t}, \tag{14}$$

where h_c is the thickness of the crushed section of the VACNT foam.

Shock velocity: The velocity at which the shock wave propagates in the VACNT foam, defined by,

$$v_s = -\frac{\Delta h_i}{\Delta t}, \tag{15}$$

where h_i is the height of the pristine section of the VACNT foam that is not compressed by the shock.

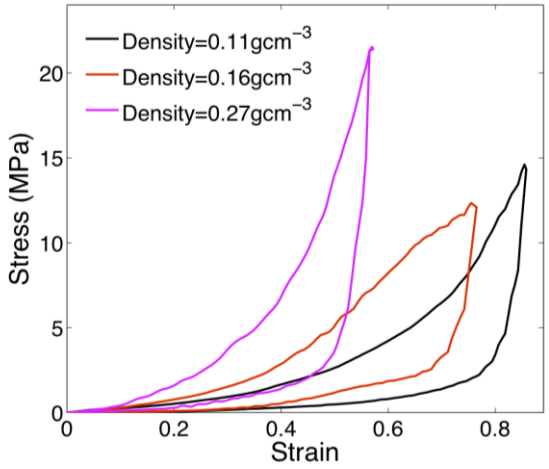

Figure S4. Characteristic dynamic stress-strain response of VACNT foams of different densities, subjected to an impact at velocity of 3.78±0.18 ms^{-1}. As the VACNT foam's density decreases the response becomes increasingly compliant with lower modulus, lower peak stress and larger deformation.

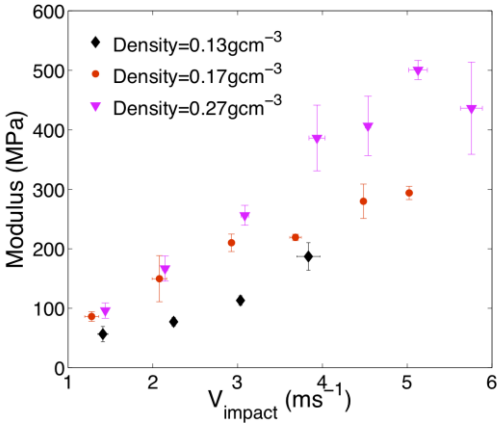

Figure S5(a). Variation of unloading modulus with impact velocity.

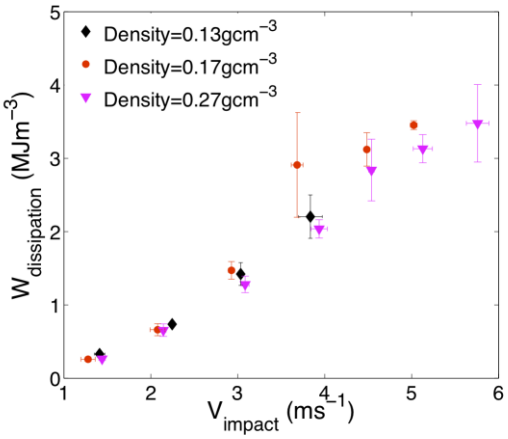

Figure S5(b). Variation of hysteretic energy dissipation with impact velocity.

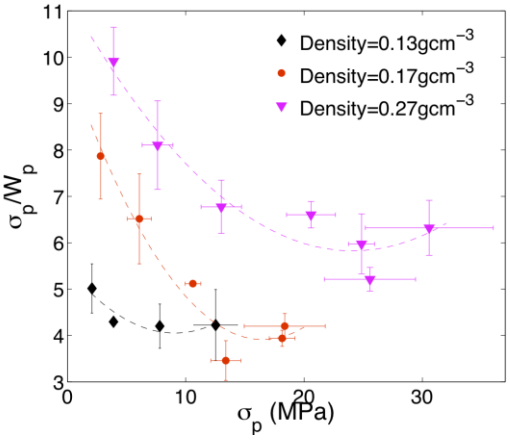

Figure S6. Variation of dynamic cushion factor with peak stress.

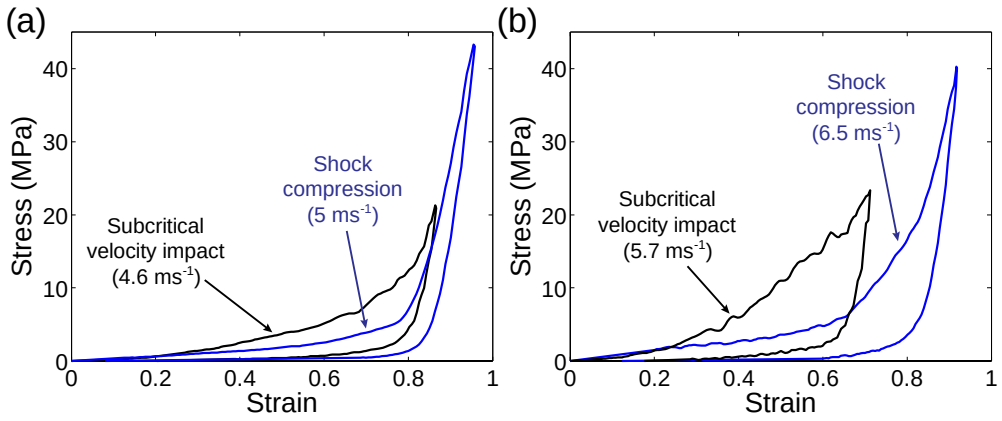

Figure S7. Comparison of dynamic stress-strain responses at subcritical velocity impact and during shock compression for **(a)** low-density VACNT foams (density ~0.12 gcm^{-3}), and **(b)** high-density VACNT foams (~0.2 gcm^{-3}). Local instabilities that are characteristic of buckle formation and progression are prominent in the subcritical responses and such a deformation response is replaced by a crush front progression during shock compression. The hysteresis also becomes narrower during shock compression compared to the hysteresis in subcritical impact velocities. The stress increases moderately up to densification, beyond which it increases rapidly reaching very high peak stresses.

References:

[1] Bedewy, M.; Meshot, E. R.; Reinker, M. J.; Hart, a J. ACS Nano 2011, 5, 8974–8989.

[2] Meshot, E.; Hart, A. Appl. Phys. Lett. 2008, 113107, 90–93.

[3] Futaba, D. N.; Hata, K.; Yamada, T.; Hiraoka, T.; Hayamizu, Y.; Kakudate, Y.; Tanaike, O.; Hatori, H.; Yumura, M.; Iijima, S. Nat. Mater. 2006, 5, 987–994.